Available online at www.sciencedirect.com
ScienceDirect
Mechanism and Machine Theory 44 (2009) 162–179
Mechanism and Machine Theory
www.elsevier.com/locate/mechmt

Kinematic and static analysis of a 3-PU$\underline{P}$S spatial tensegrity mechanism

Marc Arsenault [a,*], Clément M. Gosselin [b]

[a] *Department of Mechanical Engineering, Royal Military College of Canada, Kingston, Ontario, Canada K7K 7B4*
[b] *Départment de Génie Mécanique, Faculté des Sciences et de Génie, Université Laval, Québec, Canada G1K 7P4*

Received 11 September 2006; received in revised form 24 January 2008; accepted 10 February 2008
Available online 20 March 2008

Abstract

The development of tensegrity mechanisms is motivated by their reduced inertia which is made possible by an extensive use of cables and springs. In this paper, a new spatial tensegrity mechanism is introduced. The direct and inverse static problems of the mechanism are solved by minimizing its potential energy. For a simplified case where external and gravitational loads are neglected, analytical solutions to these problems are found and are then used to compute the boundaries of the mechanism's actuator and Cartesian workspaces.

Keywords: Tensegrity; Mechanism; Kinematic analysis; Stiffness; Workspace

1. Introduction

According to Emmerich [1], the first tensegrity structure was introduced in Russia in the early 1900s. In the middle of the 20th century, inspired by artist Kenneth Snelson's novel sculptures, Buckminster Fuller coined the word tensegrity as a combination of *tension* and *integrity* [2]. A detailed history of tensegrity systems is given by Motro [3].

The definition of tensegrity systems is not unique. A widely accepted version is proposed by Pugh [4] as follows:

> A tensegrity system is established when a set of discontinuous compressive components interacts with a set of continuous tensile components to define a stable volume in space.

The use of tensegrity systems is motivated by the fact that, as defined above, each of their components is either loaded in tension or in compression for all possible configurations. As such, cables or springs may be used for the components in tension thus greatly reducing the mass of the system. Some tensegrity systems also

* Corresponding author. Tel.: +1 613 541 6000x6622; fax: +1 613 542 8612.
E-mail addresses: marc.arsenault@rmc.ca (M. Arsenault), gosselin@gmc.ulaval.ca (C.M. Gosselin).

0094-114X/$ - see front matter © 2008 Elsevier Ltd. All rights reserved.
doi:10.1016/j.mechmachtheory.2008.02.005

have the potential to be deployable [5,6]. Such a system can thus be folded in a small volume for transportation purposes and then be erected into place by tensioning the cables. Furthermore, the use of simple and interchangeable components such as struts, cables and springs allow tensegrity systems to be cost effective and, in some cases, modular. These attributes make tensegrity systems strong candidates for space applications.

According to the tensegrity system definition, the compressive components (i.e. struts) form a discontinuous network which implies that the integrity of the system is maintained by the tensile components (i.e. cables and springs). This is made possible by the introduction of prestress in the system. A thorough explanation of the conditions required to allow a system to be prestressed is given by Pellegrino [7].

The computation of the equilibrium configuration of a tensegrity system for a given set of conditions is not a simple task. Several approaches have been proposed, mostly of numerical nature [8,9,10,11]. However, for simpler architectures [12] or when symmetrical hypotheses are made [13], analytical solutions are possible. A review of form-finding methods for tensegrity systems is given by Tibert and Pellegrino [14].

Since tensegrity systems are not rigid, the study of their stiffness is of increased importance. The stiffness of several tensegrity architectures was studied by Skelton et al. [15] while [16] developed analytical expressions for the stiffness of a prismatic tensegrity system.

Previous research on tensegrity systems has mostly concentrated on their use as adaptive structures. Among the first to propose the development of mechanisms using tensegrity principles were Oppenhein and Williams [17]. Since then, several tensegrity mechanisms have been proposed (e.g. Marshall and Crane [18]). Suggested applications include a tensegrity flight simulator [19], a tensegrity telescope [20] as well as a force and torque tensegrity sensor [21].

The development of tensegrity mechanisms is motivated by the reduced inertia of their moving parts. Furthermore, since tensegrity mechanisms are compliant, they can be useful in applications requiring a soft touch. In previous work, the authors have studied one and two degree-of-freedom planar mechanisms [22,23]. A spatial mechanism based on the triangular tensegrity prism was also developed and analysed [24]. In this paper, a new mechanism is obtained from the triangular tensegrity prism by using a different actuation scheme. From the analysis of the mechanism, observations are made with respect to its strengths and weaknesses.

2. Mechanism description

The 3-PU$\underline{P}$S tensegrity mechanism is developed from the triangular tensegrity prism shown in Fig. 1. This system consists of three struts joining node pairs A_iC_i and nine cables joining node pairs $A_iA_{i+1}, A_{i+1}C_i$ and C_iC_{i+1} (henceforth, $i = 1, 2, 3$ with $i + 1 = 1$ if $i = 3$). Reference frames $X_0Y_0Z_0$ and $X'_0Y'_0Z'_0$ are attached to the geometrical centres of nodes $A_1A_2A_3$ and $C_1C_2C_3$ as shown in Fig. 1b. It was shown by Kenner [25] that

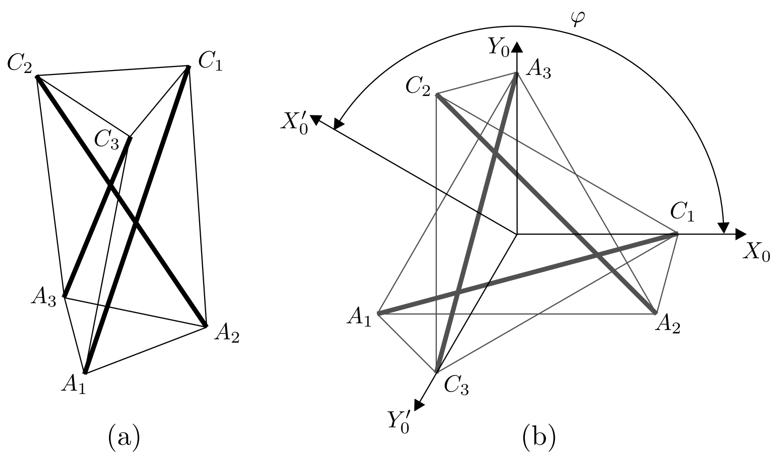

Fig. 1. Triangular tensegrity prism: (a) isometric view and (b) top view.

general prismatic tensegrity systems are in equilibrium when the rotation between their top and bottom polygons corresponds to:

$$\varphi = \frac{\pi}{2} + \frac{\pi}{\varepsilon} \tag{1}$$

where ε is the number of sides in the polygon. It follows that in the case of the triangular tensegrity prism $\varepsilon = 3$ and the rotation at equilibrium between the $X_0Y_0Z_0$ and $X'_0Y'_0Z'_0$ reference frames around axis Z_0 is equal to $\varphi = 5\pi/6$. It should also be noted that tensegrity prisms have instantaneous mobility in their equilibrium configurations. This means that infinitesimal changes in the shapes of these systems are possible without requiring deformations of their strut or cable elements. The instantaneous mobility of the triangular tensegrity prism corresponds to an infinitesimal twist of frame $X'_0Y'_0Z'_0$ relative to frame $X_0Y_0Z_0$ about the Z_0-axis.

A diagram of the 3-PU<u>P</u>S tensegrity mechanism is shown in Fig. 2a. As is the case with the triangular prismatic tensegrity system, the mechanism has three compressive and nine tensile components. The former are prismatic actuators that are used to vary the distances (ρ_i) between node pairs A_iC_i while three of the latter are cables of length L joining node pairs C_iC_{i+1}. The remaining six tensile components are springs joining node pairs A_iA_{i+1} (base springs) and $A_{i+1}C_i$ (transversal springs). The base springs have stiffness $\sqrt{3}K/3$ while the transversal springs have stiffness K. This choice of stiffnesses is made so that at equilibrium the lengths of the base springs are equal to those of the cables. Each of the springs has a length l_j $(j = 1, 2, \ldots, 6)$ and a zero-free-length. This last hypothesis is not problematic since virtual zero-free-length springs can be created by extending the actual springs beyond their attachment points [26]. Examples of this are given in Ref. [27]. Finally, it should be noted that the stiffnesses of the actuators and cables are assumed to be infinite relative to those of the springs.

The mechanism's A_i nodes are free to translate along passive prismatic joints that are symmetrically distributed in a plane as shown in Fig. 2b. The position of node A_i along its passive prismatic joint is denoted by ξ_i. A fixed reference frame XYZ, whose origin is used to represent the mechanism's base, is attached to the point of intersection of the passive prismatic joints with its Y-axis directed towards node A_3 and its Z-axis perpendicular to the plane formed by nodes $A_1A_2A_3$. Meanwhile, a mobile reference frame $X'Y'Z'$ representing the mechanism's effector is defined as being attached to the geometric centre of nodes $C_1C_2C_3$ with its Y-axis directed towards node C_3 and its Z-axis perpendicular to the plane formed by nodes $C_1C_2C_3$. Finally, the prismatic actuators are connected to nodes A_i by passive universal joints and to the cables at nodes C_i by passive spherical joints. It can be mentioned, however, that these spherical joints may be omitted because of the cables' flexibility.

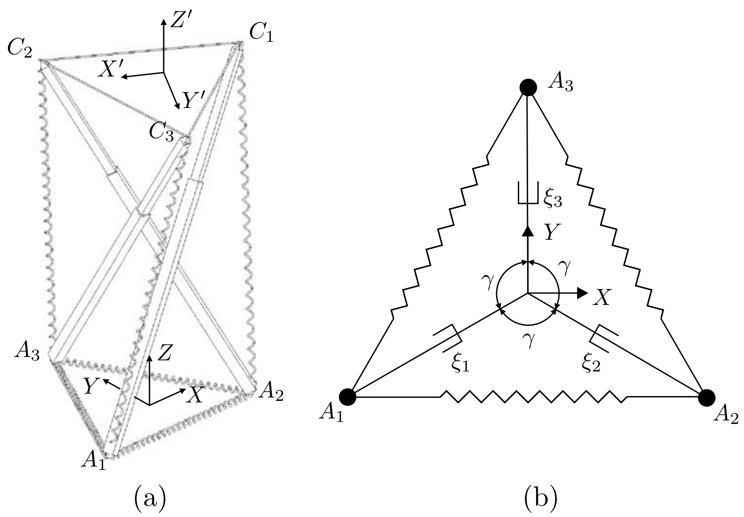

Fig. 2. 3-PU<u>P</u>S tensegrity mechanism: (a) general view and (b) base architecture.

Referring once again to Fig. 2b, vectors defining the positions of nodes A_i in frame XYZ are defined as:

$$\boldsymbol{a}_1 = \begin{bmatrix} -\xi_1 \sin(\gamma/2) \\ -\xi_1 \cos(\gamma/2) \\ 0 \end{bmatrix} \quad \boldsymbol{a}_2 = \begin{bmatrix} \xi_2 \sin(\gamma/2) \\ -\xi_2 \cos(\gamma/2) \\ 0 \end{bmatrix} \quad \boldsymbol{a}_3 = \begin{bmatrix} 0 \\ \xi_3 \\ 0 \end{bmatrix} \tag{2}$$

with $\gamma = 2\pi/3$. In order to compute position vectors for nodes C_i, XZ Euler angles are used to define the rotations of the universal joints with the actuators assumed to be initially parallel to the Y-axis. Unit vectors directed along the actuators' longitudinal axes are thus expressed as:

$$\boldsymbol{e}_i = [-\sin\beta_i,\ \cos\alpha_i\cos\beta_i,\ \sin\alpha_i\cos\beta_i]^{\mathrm{T}} \tag{3}$$

where α_i and β_i represent the rotations about the Euler angle X and Z axes (not to be confounded with the axes of the XYZ frame), respectively. Using this definition, the positions of nodes C_i are obtained as:

$$\boldsymbol{c}_i = \boldsymbol{a}_i + \rho_i \boldsymbol{e}_i \tag{4}$$

It will henceforth be assumed that the springs and cables are massless. Furthermore, both the prismatic actuator sleeve and core will be assumed to have length L_p and mass m with the positions of their centres of gravity expressed as (see Fig. 3):

$$\boldsymbol{p}_{s_i} = \boldsymbol{a}_i + \frac{L_p}{2}\boldsymbol{e}_i \quad \boldsymbol{p}_{c_i} = \boldsymbol{a}_i + \left(\rho_i - \frac{L_p}{2}\right)\boldsymbol{e}_i \tag{5}$$

with gravity acting in the negative direction of the Z-axis.

The mobility of the mechanism can be analysed using the well-known Chebychev–Grübler–Kutzbach formula [28]. In order to facilitate this analysis, it is useful to view the cables joining node pairs C_iC_{i+1} as being replaced with a triangular plate to which the actuators are connected with spherical joints. In fact, such a replacement is feasible in practice since the cables are always subjected to tension which implies that the shape and size of the triangle formed by nodes C_i do not change. Furthermore, this does not alter in any way the mobility of the mechanism. Additionally, the springs need not be considered for this analysis since they do not constrain the mechanism. The mobility graph of the mechanism is thus drawn in Fig. 4. From this figure, it can be observed that the mechanism has 11 rigid bodies ($n = 11$) and 12 joints ($g = 12$) whose degrees of freedom are $f_k = 1$ if the joint is prismatic, $f_k = 2$ if it is universal and $f_k = 3$ if it is spherical. Substituting these values into the mobility formula yields the following:

$$l = 6(n - g - 1) + \sum_{k=1}^{g} f_k = 6(11 - 12 - 1) + 21 = 9 \tag{6}$$

The mechanism has nine degrees of freedom of which three are removed when the lengths of the prismatic actuators are fixed. This leaves six degrees of freedom that are unconstrained. For given positions of the actuators, these unconstrained degrees of freedom are driven by the need for the mechanism to minimize its potential energy. By modifying the lengths of the actuators, it is possible to modify the configuration where the

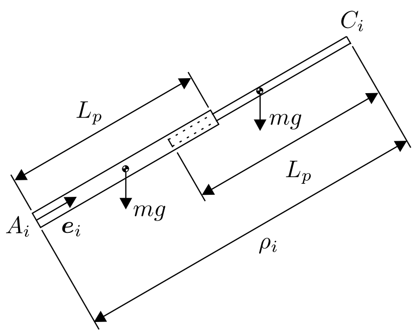

Fig. 3. Detailed view of the mechanism's prismatic actuator.

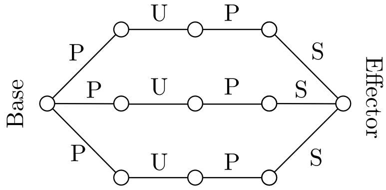

Fig. 4. Mobility graph.

equilibrium of the mechanism occurs with three degrees of freedom. In this work, these controlled degrees of freedom will be chosen as the position coordinates of the mechanism's effector in the Cartesian space. The output vector of the mechanism is thus the position of frame $X'Y'Z'$ with respect to frame XYZ expressed as:

$$\boldsymbol{x} = [x, y, z]^{\mathrm{T}} \tag{7}$$

while its input vector corresponds to the lengths of the prismatic actuators:

$$\boldsymbol{\psi} = [\rho_1, \rho_2, \rho_3]^{\mathrm{T}} \tag{8}$$

The following vector of generalized coordinates represents the unconstrained degrees of freedom of the mechanism:

$$\boldsymbol{q} = [\xi_1, \xi_2, \xi_3, \alpha_1, \beta_1, \alpha_2, \beta_2, \alpha_3, \beta_3]^{\mathrm{T}} \tag{9}$$

of which three are superfluous. In addition to vectors $\boldsymbol{\psi}$ and $\boldsymbol{q}$, the following three geometric constraints associated to the lengths of the cables must be used to completely define the mechanism's configuration:

$$\phi_i = (\boldsymbol{c}_i - \boldsymbol{c}_{i+1})^{\mathrm{T}}(\boldsymbol{c}_i - \boldsymbol{c}_{i+1}) - L^2 = 0 \tag{10}$$

A vector of constraints is defined as $\boldsymbol{\phi} = [\phi_1, \phi_2, \phi_3]^{\mathrm{T}}$.

3. Kinematic and static analysis – general case

Unlike conventional mechanisms, the movement of a tensegrity mechanism depends not only on its actuator positions but also on any external, gravitational or inertial loads that might be acting on it. This is due to the presence of unconstrained degrees of freedom in these mechanisms. In this section, it is always assumed that the 3-PU$\underline{\text{P}}$S mechanism is in static equilibrium. With this assumption, the behaviour of the mechanism is analysed while considering both its kinematic and static properties.

3.1. Direct static problem

The direct static problem of a tensegrity mechanism is defined as the computation of its output variables ($\boldsymbol{x}$) for a given set of actuator positions ($\boldsymbol{\psi}$) when subjected to external loads. By nature, tensegrity mechanisms will always deform so as to minimize their potential energy. The solution to the direct static problem of the mechanism is based on this fact. The potential energy of the 3-PU$\underline{\text{P}}$S mechanism is expressed as follows:

$$U = \frac{1}{2}K\left(\frac{\sqrt{3}}{3}\sum_{j=1}^{3} l_j^2 + \sum_{j=4}^{6} l_j^2\right) + mg\boldsymbol{e}_g^{\mathrm{T}}\sum_{i=1}^{3}(\boldsymbol{p}_{s_i} + \boldsymbol{p}_{c_i}) \tag{11}$$

where the spring lengths are computed as:

$$l_i^2 = (\boldsymbol{a}_{i+1} - \boldsymbol{a}_i)^{\mathrm{T}}(\boldsymbol{a}_{i+1} - \boldsymbol{a}_i), \quad l_{i+3}^2 = (\boldsymbol{c}_i - \boldsymbol{a}_{i+1})^{\mathrm{T}}(\boldsymbol{c}_i - \boldsymbol{a}_{i+1}) \tag{12}$$

and $\boldsymbol{e}_g = [0, 0, 1]^{\mathrm{T}}$ is a vector directed along the negative direction of gravity (i.e. along the positive Z-axis). In order to solve the direct static problem of the mechanism, it is sought to minimize U with respect to the generalized coordinates while ensuring the satisfaction of the geometric constraints (Eq. (10)). External forces are also assumed to be acting on nodes C_1, C_2 and C_3. The following function is thus defined:

$$\eta = U - \sum_{i=1}^{3} \boldsymbol{f}_i^{\mathrm{T}} \boldsymbol{c}_i + \boldsymbol{\lambda}^{\mathrm{T}} \phi \tag{13}$$

where $\boldsymbol{f}_i$ is an external force applied to node C_i and $\boldsymbol{\lambda}$ is a vector of Lagrange multipliers used to apply the constraints. In order for the mechanism to be in a static equilibrium for given actuator positions and external forces, the following conditions must be satisfied:

$$\frac{\partial \eta}{\partial \boldsymbol{q}} = \boldsymbol{0} \quad \frac{\partial \eta}{\partial \boldsymbol{\lambda}} = \boldsymbol{0} \tag{14}$$

These conditions, which are associated to critical points of η, correspond to a non-linear system of 12 scalar equations in 12 unknowns. Because of its complexity, this system must be solved for $\boldsymbol{q}$ with a numerical approach such as the Newton–Raphson algorithm. However, solutions to the above system of equations that are computed with this algorithm do not necessarily correspond to stable equilibrium configurations of the mechanism. Consequently, a continuation approach is used in order to proceed with small steps from a reference configuration that is known to correspond to a stable equilibrium to the final sought configuration. Starting from a reference configuration defined by $\boldsymbol{\psi}_0, \boldsymbol{f}_1 = \boldsymbol{f}_2 = \boldsymbol{f}_3 = \boldsymbol{0}$ and $g = 0$, the line joining $\boldsymbol{\psi}_0$ and $\boldsymbol{\psi}$ in the actuator space is first discretized into a set of increments. The Newton–Raphson algorithm is then used to solve the system of Eq. (14) for each of these increments using the solution of the previous increment as the initial guess for the subsequent computation. Once the system has been solved for $\boldsymbol{\psi}$, a second continuation phase is used where the external and gravitational forces are gradually applied leading to the final sought configuration. Once the set of generalized coordinates corresponding to given actuator positions and external forces has been found, the output of the mechanism can be computed as:

$$\boldsymbol{x} = \frac{1}{3} \sum_{i=1}^{3} \boldsymbol{c}_i \tag{15}$$

3.2. Inverse static problem

The inverse static problem of a tensegrity mechanism is defined here as the computation of the set of actuator positions ($\boldsymbol{\psi}$) required for the mechanism's effector to be in a given position ($\boldsymbol{x}$) when it is subjected to a given set of external loads ($\boldsymbol{f}_i$). In order to solve the inverse static problem of the 3-PU<u>P</u>S mechanism, its potential energy (Eq. (11)) must be minimized with respect to $\boldsymbol{q}$ as was the case for the direct static problem. However, the mechanism's actuator positions are now considered as unknowns. The conditions expressed by Eq. (14) thus represent a system of 12 equations in 15 unknowns. In addition, the following constraint equations pertaining to the desired position of the mechanism's effector must also be satisfied as per the problem definition:

$$\boldsymbol{x} - \frac{1}{3} \sum_{i=1}^{3} \boldsymbol{c}_i = \boldsymbol{0} \tag{16}$$

These three scalar equations combined with the original system of equations yield a non-linear system that can be solved once again with the Newton–Raphson algorithm. A continuation approach similar to the one described in Section 3.1 is used in order to ensure that the solution that is found corresponds to a stable equilibrium configuration.

3.3. Allowable set of external forces

Since tensegrity mechanisms have unconstrained degrees of freedom, they will deform under the application of external loads. However, there exists a limit to the extent with which the mechanisms can resist to these loads. The aim of this section is to compute the sets of external loads that can be sustained by the 3-PU<u>P</u>S mechanism.

When solving the direct and inverse static problems, external forces were assumed to be acting directly on nodes C_i. Since nine variables must be used to represent the state of the external loading in such a situation, the analysis of the resulting set of allowable external forces would be very onerous. For this reason, a tripod is attached to the mechanism's effector in order to apply a single external force that can be represented by three parameters. The tripod is formed by three struts of length L that are connected at one end to nodes C_i and are joined together at their opposite ends with spherical joints. By applying an external force $\boldsymbol{f}_T$ at the top vertex of the tripod, a unique set of equivalent forces $\boldsymbol{f}_i$ acting at nodes C_i can be computed. These can then be used in the direct static problem to compute the equilibrium of the mechanism for the given force.

The first step used to compute the allowable set of external forces consists in discretizing the three-dimensional external force space. Angles v_1 and v_2 are used to represent the direction of $\boldsymbol{f}_T$ while $\|\boldsymbol{f}_T\|$ represents its magnitude. An expression for $\boldsymbol{f}_T$ is thus obtained as:

$$\boldsymbol{f}_T = \|\boldsymbol{f}_T\|[\cos v_1 \cos v_2,\ \sin v_1 \cos v_2,\ \sin v_2]^{\mathrm{T}} \tag{17}$$

A radial discretization is used where for a given direction of $\boldsymbol{f}_T$ defined by v_1 and v_2 its magnitude is divided into increments. For a given set of actuator positions, the largest magnitude of $\boldsymbol{f}_T$ that can be supported by the mechanism is computed for each direction. This is done by incrementing $\|\boldsymbol{f}_T\|$ upwards from zero until one of the following three conditions is violated:

(1) The cables are in tension.
(2) The prismatic actuators are in compression.
(3) The mechanism's equilibrium configuration evolves smoothly and remains stable for smooth increments of $\|\boldsymbol{f}_T\|$.

The first two of these conditions are self-explanatory. Further detail will now be given regarding the third condition. It is expected that when an external force is applied smoothly to the mechanism using increments, the latter should deform in a smooth fashion as the critical point of its η function that is associated to its equilibrium is displaced. However, in certain situations, incrementing the amplitude of the external force leads to a drastic change in the mechanism's equilibrium configuration. This phenomenon is caused by a qualitative change in the η function of the mechanism where the critical point previously associated to the mechanism's equilibrium disappears. Because of this, the mechanism quickly moves to a new equilibrium. Such behaviour must obviously be avoided and so this condition represents a boundary of the allowable external forces set.

At each increment of $\|\boldsymbol{f}_T\|$ in a given direction, the direct static problem is solved. The first two conditions are then verified by computing the loads in the mechanism's components while a violation of the third condition is identified when the algorithm used to solve the direct static problem fails to converge on a solution. The boundary surface of the set of allowable external forces is obtained by plotting the maximum values of $\|\boldsymbol{f}_T\|$ not violating the constraints for each direction. An example of this boundary is shown in Fig. 5 for

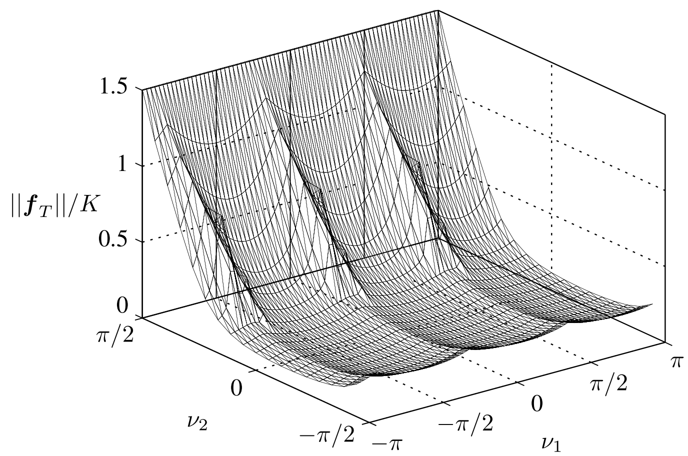

Fig. 5. Set of allowable external forces for the case where $L = \sqrt{2}/2$ and $\boldsymbol{\psi} = [2, 2, 2]^{\mathrm{T}}$.

$-\pi < v_1 \leqslant \pi$ and $-\pi/2 < v_2 \leqslant \pi/2$. In this figure, $\|\boldsymbol{f}_T\|$ has been normalized relative to the stiffness of the mechanism's springs. It can be seen that larger external forces can be applied to the mechanism along the positive Z-axis (i.e. when v_2 approaches $\pi/2$). Furthermore, the surface is symmetric with respect to the directions of the A_i nodes' passive prismatic actuators (i.e. $v_1 = -5\pi/6, -\pi/6$ and $\pi/2$). The case where $v_2 = -\pi/2$ is excluded from the set. In fact, a value of $\|\boldsymbol{f}_T\|/K \approx 3.3$ can be sustained in the downwards direction. However, for the configuration considered here, the mechanism becomes unstable in such a situation since a slight deviation of the external force direction will lead to a collapse. This behaviour can be compared to that of a beam in compression that might buckle if the direction of the compressive force deviates slightly from the beam's centre axis.

3.4. Stiffness

The ability of a mechanism to resist to deformations under the application of external loads is quantified by its stiffness. The latter is an important performance indicator for tensegrity mechanisms because of the inherent potential for deformations related to their unconstrained degrees of freedom. In what follows, external forces are assumed to be acting directly on nodes C_1, C_2 and C_3. As a consequence, the stiffness of the 3-PU$\underline{\text{P}}$S mechanism will need to be computed separately for each of these nodes. Furthermore, since the stiffness is a configuration and direction dependent property, it will need to be computed for given equilibrium configurations as well as for specific directions which in this case will be chosen as the X, Y and Z axes of the fixed reference frame.

In the following, the stiffness analysis will be restricted to equilibrium configurations where no external or gravitational forces are acting. Because of the complexity of the mechanism's behaviour, a numerical approximation of the stiffness will be used. The procedure used for this approximation consists of the following steps where, for illustrative purposes, it is assumed that the stiffness of node C_1 along the X-axis is being computed.

(1) The equilibrium configuration of the mechanism for a given set of actuator positions ($\boldsymbol{\psi}$) is computed where external and gravitational forces are set to zero.
(2) Small external forces of magnitude $\pm\delta f$ are applied to node C_1 along the X-axis while keeping the actuator positions fixed. The two resulting equilibrium configurations are found by solving the direct static problem of the mechanism.
(3) The displacement of node C_1 along the X-axis between the above equilibrium configurations corresponding to $\pm\delta f$ is computed as $\Delta c_{1,x}$.
(4) The stiffness at node C_1 along the X-axis ($K_{C_1,x}$), which mathematically corresponds to the slope of the profile of an external force applied at C_1 along the X-axis versus the corresponding displacement of C_1 along X, is approximated (see Eq. 18).

The computation of the stiffness as described in step 4 above is accomplished for an arbitrary C_i node along any Cartesian axis using the following equations where the stiffness has been normalized relative to the stiffness of the mechanism's springs:

$$K_{C_i,x} = \frac{2\delta f}{K\Delta c_{i,x}} \quad K_{C_i,y} = \frac{2\delta f}{K\Delta c_{i,y}} \quad K_{C_i,z} = \frac{2\delta f}{K\Delta c_{i,z}} \tag{18}$$

As a consequence of the non-linear deformations of the mechanism under the application of external loads, δf must be kept relatively small in order to compute the stiffness with greater accuracy (in this work $\delta f = K/1000$ is used).

With the goal of analyzing the mechanism's stiffness for different configurations, stiffness mappings are generated in the Cartesian space (see Fig. 6). Since the representation of these mappings is two-dimensional, constant values of z are used. However, although it is not done here, the value of z can easily be varied to obtain a series of mappings that represent the entire Cartesian space. As can be seen in Fig. 6, the mappings are limited to areas which correspond to the mechanism's Cartesian workspace. The boundaries of this workspace are detailed in Section 4.6. Finally, the stiffness mappings are generated specifically for the C_1 node. However,

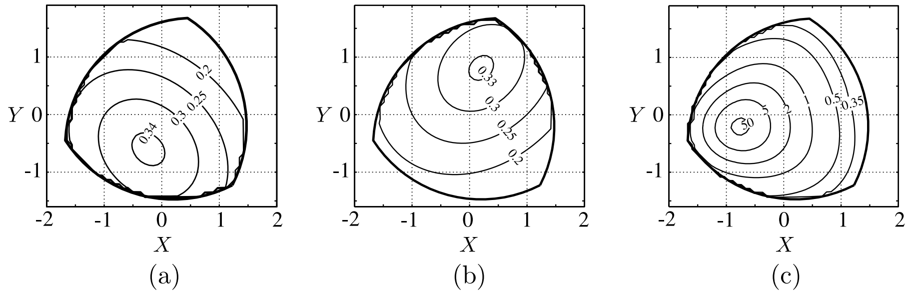

Fig. 6. Stiffness distribution at node C_1 for $z = 2$ and $L = \sqrt{2}/2$: (a) $K_{C_1,x}$, (b) $K_{C_1,y}$ and (c) $K_{C_1,z}$.

because of the mechanism's symmetry, it can be shown that its stiffness mappings at nodes C_2 and C_3 are equivalent.

Observing Fig. 6, it can be seen that in each of the mappings the stiffness of the mechanism has a distinct maximum value. In order to understand these maximum stiffness configurations, physical justifications must be found to explain why one particular configuration is stiffer than another. With this goal in mind, the stiffness of the mechanism is computed in all directions for a given node and a given configuration. The resulting stiffness distribution can then be plotted as a volume that encompasses the node of interest. An example of this is shown in Fig. 7 where the stiffness at node C_1 was computed in every possible direction for a configuration where $\boldsymbol{\psi} = [2, 2, 2]^{\mathrm{T}}$ and $\boldsymbol{x} = [0, 0, 2]^{\mathrm{T}}$. From this figure, the principal stiffness directions can be found. These correspond to the directions of maximum ($\boldsymbol{e}_{\max}$) and minimum ($\boldsymbol{e}_{\min}$) stiffness as well as an intermediate direction ($\boldsymbol{e}_{\mathrm{int}}$) that is perpendicular to the plane defined by the first two. The orientation of the line joining nodes A_1 and C_1, which corresponds to the compression axis of the prismatic actuator, is also shown ($\boldsymbol{e}_{A_1-C_1}$). By repeating this process for different configurations as well as for different C_i nodes, a link between the principal stiffness directions and the arrangement of the mechanism's components becomes apparent. For a given configuration, the stiffness at node C_i is maximum (minimum) in a direction that tends to minimize (maximize) two quantities. The first quantity is the moment generated on the actuator about node A_i by an external force applied at node C_i (this moment is zero when the external force is directed along the line joining nodes A_i and C_i). The second quantity is the component of this same external force that is parallel to the passive prismatic actuator on which node A_i is free to translate. The direction of maximum stiffness is a compromise between the

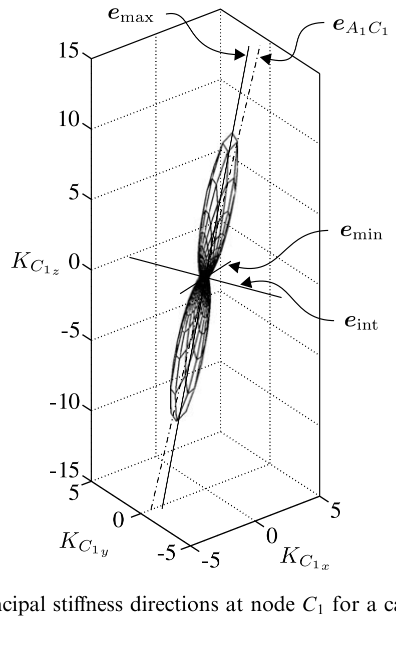

Fig. 7. Stiffness distribution and principal stiffness directions at node C_1 for a case where $\boldsymbol{x} = [0, 0, 2]^{\mathrm{T}}$ and $L = \sqrt{2}/2$.

directions minimizing theses two quantities with most of the emphasis being placed on the first. In fact, as shown in Fig. 7, $\boldsymbol{e}_{\max}$ and $\boldsymbol{e}_{A_1C_1}$ are very close to being parallel.

Using the above developments, the maximum stiffness configuration along the Z-axis ($K_{C_1,z}$) can be explained in a straightforward manner (see Fig. 6c). In fact, this configuration simply corresponds to a situation where the line joining nodes A_1 and C_1 is parallel to the Z-axis. When this is the case, an external force applied at C_1 along the Z-axis passes through node A_1 and so does not generate a moment relative to this node. Furthermore, such a force does not have a component parallel to node A_1's passive prismatic actuator since the latter is located in the XY plane. It follows that in such a configuration the stiffness of the mechanism at node C_1 in the Z-axis direction is infinite. For the stiffness of the mechanism along the X and Y axes, the configurations of maximum stiffness for given slices of the Cartesian workspace (i.e. $z =$ constant) are those where the distances along axes $K_{C1,x}$ and $K_{C1,y}$ from the origin to the boundary of the surface volume are greatest. This depends not only on the principal stiffness directions but also on their magnitudes (e.g. Fig. 7).

The observations made thus far regarding the stiffness of the mechanism were based on Cartesian stiffness mappings where $z = 2$. When the z coordinate is varied, the qualitative behaviour of the mechanism's stiffness do not change. However, as z is reduced, the stiffness of the mechanism along the Z-axis also diminishes globally until they become zero when $z = 0$. It should however be noted that locally the stiffness of the mechanism along the Z-axis at nodes C_i is always infinite when the line joining nodes A_i and C_i is parallel to the Z-axis. In the case of the stiffness along the X and Y axes, there is an increase for decreasing z since the line joining nodes A_i and C_i progressively approaches the XY plane.

4. Kinematic and static analysis – special case

In the previous section, the kinematic and static analysis of the 3-PU$\underline{\text{P}}$S mechanism was performed for a completely general case. In this section, a special case is considered where external and gravitational forces are neglected. It is shown that, under such conditions, the analysis of the mechanism leads to analytical results.

4.1. Direct static problem

When the direct static problem of the mechanism is solved numerically using the method described in Section 3.1 while neglecting external and gravitational forces, it is observed that for any given set of actuator positions the equilibrium configuration of the mechanism corresponds to a pure translation of its effector. Furthermore, the mechanism's A_i nodes are always positioned such that $\xi_1 = \xi_2 = \xi_3 = \sqrt{3}L/3$ which implies that the distances between node pairs A_iA_{i+1} are equal to the length of the cables joining nodes C_iC_{i+1} (i.e. L). Assuming these observations to be valid for all $\boldsymbol{\psi}$ (this will be proven in Section 4.8), an analytical solution to the direct static problem of the mechanism is computed as follows.

Position vectors for nodes C_i relative to the effector frame are given by:

$$\boldsymbol{s}'_1 = \begin{bmatrix} -L/2 \\ -\sqrt{3}L/6 \\ 0 \end{bmatrix} \quad \boldsymbol{s}'_2 = \begin{bmatrix} L/2 \\ -\sqrt{3}L/6 \\ 0 \end{bmatrix} \quad \boldsymbol{s}'_3 = \begin{bmatrix} 0 \\ \sqrt{3}L/3 \\ 0 \end{bmatrix} \tag{19}$$

where the $'$ symbol denotes vectors expressed in the $X'Y'Z'$ frame. Furthermore, according to the observations made in the preceding paragraph, $\boldsymbol{a}_i = \boldsymbol{s}'_i$. This is to say that the triangle formed by nodes $A_1A_2A_3$ is congruent to the one formed by nodes $C_1C_2C_3$. The direct static problem of the mechanism can thus be solved by computing the intersection of spheres of radii ρ_i expressed as

$$(\boldsymbol{x} - \boldsymbol{a}_i + \mathbf{Q}_e\boldsymbol{s}'_i)^{\mathrm{T}}(\boldsymbol{x} - \boldsymbol{a}_i + \mathbf{Q}_e\boldsymbol{s}'_i) - \rho_i^2 = 0 \tag{20}$$

where

$$\mathbf{Q}_e = \begin{bmatrix} \cos\varphi & -\sin\varphi & 0 \\ \sin\varphi & \cos\varphi & 0 \\ 0 & 0 & 1 \end{bmatrix} \tag{21}$$

with $\varphi = 5\pi/6$. Solving the system represented by Eq. (20) yields:

$$x = \frac{\sqrt{3}}{6L}\left[\rho_1^2 + \left(1-\sqrt{3}\right)\rho_2^2 + \left(\sqrt{3}-2\right)\rho_3^2\right] \tag{22}$$

$$y = \frac{2\sqrt{3}-3}{6L}\left[\rho_1^2 + \left(1+\sqrt{3}\right)\rho_2^2 - \left(2+\sqrt{3}\right)\rho_3^2\right] \tag{23}$$

$$z = \frac{\sqrt{3(2-\sqrt{3})S_1}}{3L} \tag{24}$$

with:

$$S_1 = \left(2+\sqrt{3}\right)L^2\sum_{i=1}^{3}\rho_i^2 - \sum_{i=1}^{3}\rho_i^4 + \rho_1^2\rho_2^2 + \rho_1^2\rho_3^2 + \rho_2^2\rho_3^2 - \left(7+4\sqrt{3}\right)L^4 \tag{25}$$

It can be noted that the square root appearing in Eq. (24) is always taken to be positive. However, as can be seen, the direct static problem of the mechanism theoretically has two solutions that are symmetric relative to the XY plane.

4.2. Inverse static problem

From Eq. (20), the inverse static problem of the 3-PU̲PS mechanism can be solved as follows:

$$\rho_1 = \sqrt{\left[x + \left(\frac{2\sqrt{3}+3}{6}\right)L\right]^2 + \left[y + \frac{\sqrt{3}}{6}L\right]^2 + z^2} \tag{26}$$

$$\rho_2 = \sqrt{\left[x - \left(\frac{\sqrt{3}+3}{6}\right)L\right]^2 + \left[y + \left(\frac{\sqrt{3}+3}{6}\right)L\right]^2 + z^2} \tag{27}$$

$$\rho_3 = \sqrt{\left[x - \frac{\sqrt{3}}{6}L\right]^2 + \left[y - \left(\frac{2\sqrt{3}+3}{6}\right)L\right]^2 + z^2} \tag{28}$$

where the square roots are always taken to be positive since $\rho_i \geqslant 0$.

4.3. Jacobian matrices

For conventional mechanisms, Jacobian matrices are often used to establish linear relationships between input and output velocities. Because of its unconstrained degrees of freedom, this is generally not possible for the 3-PU̲PS mechanism. However, if a quasi-static state is assumed, Jacobian matrices can be used to relate infinitesimal changes in the mechanism's actuator positions ($\delta\boldsymbol{\psi}$) to corresponding infinitesimal movements of its effector ($\delta\boldsymbol{x}$). The resulting relationships can then be analysed to identify special cases where they degenerate. It will be shown in subsequent sections that these special cases correspond to the workspace boundaries of the mechanism. Using the analytical solutions of the mechanism's direct and inverse static problems, direct and inverse Jacobian matrices ($\mathbf{J}_\mathrm{D}$ and $\mathbf{J}_\mathrm{I}$) linking $\delta\boldsymbol{\psi}$ and $\delta\boldsymbol{x}$ are now computed. The direct Jacobian matrix $\mathbf{J}_\mathrm{D}$ relates $\delta\boldsymbol{x}$ to $\delta\boldsymbol{\psi}$ such that:

$$\delta\boldsymbol{x} = \mathbf{J}_\mathrm{D}\delta\boldsymbol{\psi} \tag{29}$$

and can be computed as follows:

$$\mathbf{J}_\mathrm{D} = \frac{\partial\boldsymbol{x}}{\partial\boldsymbol{\psi}} \tag{30}$$

from Eqs. (22)–(24). The elements of $\mathbf{J}_\mathrm{D}$ are thus written in terms of the actuator lengths. In order to simplify the analysis of the singular configurations, $\mathbf{J}_\mathrm{D}$ can be decomposed into matrices $\mathbf{A}$ and $\mathbf{B}$ such that:

$$\mathbf{A}\delta\boldsymbol{x} = \mathbf{B}\delta\boldsymbol{\psi} \tag{31}$$

Conversely, the inverse Jacobian matrix $\mathbf{J}_{\mathrm{I}}$ relates $\delta\boldsymbol{\psi}$ to $\delta\boldsymbol{x}$ such that:

$$\delta\boldsymbol{\psi} = \mathbf{J}_{\mathrm{I}}\delta\boldsymbol{x} \tag{32}$$

and is computed as follows:

$$\mathbf{J}_{\mathrm{I}} = \frac{\partial\boldsymbol{\psi}}{\partial\boldsymbol{x}} \tag{33}$$

from Eqs. (26)–(28). The elements of $\mathbf{J}_{\mathrm{I}}$ are thus written as a function of the Cartesian coordinates of the mechanism's end-effector. As was done with the direct Jacobian matrix, $\mathbf{J}_{\mathrm{I}}$ can be decomposed in two matrices $\mathbf{C}$ and $\mathbf{D}$ such that:

$$\mathbf{C}\delta\boldsymbol{\psi} = \mathbf{D}\delta\boldsymbol{x} \tag{34}$$

In order to alleviate the text, the elements of the direct and inverse Jacobian matrices will not be detailed here.

4.4. Singular configurations

The singular configurations of tensegrity mechanisms are defined as those where the relationships between infinitesimal movements of the actuators and of the effector degenerate. When such a situation occurs, the mechanism will either gain or lose one or more degrees of freedom thus leading to a loss of controllability. As a consequence, such configurations are usually avoided when possible. The conditions required for singular configurations to occur in the actuator space are expressed as follows:

$$\det\mathbf{A} = 27\left(\sqrt{3}-1\right)L^3\sqrt{S_1} = 0 \tag{35}$$

$$\det\mathbf{B} = 54\sqrt{2}\left(2-\sqrt{3}\right)L^2\rho_1\rho_2\rho_3 = 0 \tag{36}$$

Similarly, the conditions required for singular configurations to occur in the Cartesian space are as follows:

$$\det\mathbf{C} = P_1P_2P_3 = 0 \tag{37}$$

$$\det\mathbf{D} = \frac{27}{2}(2\sqrt{3}+3)L^2z = 0 \tag{38}$$

where P_1, P_2 and P_3 correspond to the right hand sides of Eqs. (26)–(28), respectively. In terms of physical meaning, it can be noted that the conditions expressed by Eqs. (35) and (38) are equivalent as are those expressed by Eqs. (36) and (37). The difference between these conditions is simply the space in which they are defined (i.e. actuator or Cartesian). From Eqs. (35)–(38), the following singular configurations can be identified:

(i) $S_1 = 0 \mid z = 0$
- All of the mechanism's components are located in the XY plane.
- Infinitesimal movements of nodes C_i along the Z-axis are possible with the actuators locked and without requiring deformations of the springs.
- The two theoretical solutions to the mechanism's direct static problem meet (see Section 4.1).

(ii) $\rho_1 = 0,\ \rho_2 = \rho_3 = \frac{\sqrt{2}}{2}(1+\sqrt{3})L$ or $x = -\frac{(2\sqrt{3}+3)}{6}L,\ y = -\frac{\sqrt{3}}{6}L,\ z = 0(P_1 = 0)$
- All of the mechanism's components are located in the XY plane.
- Nodes A_1 and C_1 are superimposed.
- Infinitesimal movements of nodes C_2 and C_3 along the Z-axis are possible with the actuators locked and without requiring deformations of the springs.
- $S_1 = 0$.
- The two theoretical solutions to the mechanism's direct static problem meet.

(iii) $\rho_2 = 0,\ \rho_1 = \rho_3 = \frac{\sqrt{2}}{2}(1+\sqrt{3})L$ or $x = \frac{(\sqrt{3}+3)}{6}L,\ y = -\frac{(\sqrt{3}+3)}{6}L,\ z = 0\ (P_2 = 0)$
   – Same as singular configuration (ii) with appropriate changes to the node indices.

(iv) $\rho_3 = 0,\ \rho_1 = \rho_2 = \frac{\sqrt{2}}{2}\left(1+\sqrt{3}\right)L | x = \frac{\sqrt{3}}{6}L,\ y = \frac{(2\sqrt{3}+3)}{6}L,\ z = 0\ (P_3 = 0)$
   – Same as singular configuration (ii) with appropriate changes to the node indices.

4.5. Actuator workspace

The actuator workspace of a tensegrity mechanism is defined as the region of the actuator space where the mechanism can operate. For the 3-PUPS mechanism, the boundary of the theoretical actuator workspace corresponds to singular configuration (i) of Section 4.4. This actuator workspace is referred to as theoretical since it does not consider the limited operating ranges of the actuators. An example of the theoretical actuator workspace is shown in Fig. 8. It consists of a tube-like volume whose boundary is defined by $S_1 = 0$. Although it is not easily visible in Fig. 8 the volume is an open set in the actuator space. In other words, the volume of the theoretical actuator workspace is infinite. However, in a practical setting, the prismatic actuators are limited to operating ranges defined by $\rho_{i,\min} \leqslant \rho_i \leqslant \rho_{i,\max}$. These operating ranges correspond to a cube in the actuator space whose intersection with the theoretical actuator workspace yields the actual actuator workspace which is not shown here. It can also be seen in Fig. 8 that the bottom end of the tube-like volume contains three vertices. These correspond to singular configurations (ii) through (iv) of Section 4.4.

4.6. Cartesian workspace

From singular configuration (i) of Section 4.4, it can be seen that the mapping to Cartesian space of the surface defined by $S_1 = 0$ in the 3-PUPS mechanism's actuator space simply leads to the XY plane (i.e. $z = 0$). This implies that the theoretical Cartesian workspace of the mechanism corresponds to the entire Cartesian space minus the XY plane where the mechanism is in a singular configurations. Obviously this is not true in practice since the operating ranges of the actuators are limited. When these limits are considered, the workspace of the mechanism can be computed with the same approach that is used to determine the constant orientation workspace of the well-known Stewart–Gough platform [29]. In order to do this, the ρ_i appearing in Eqs. (26)–(28) are successively replaced with specified values of $\rho_{i,\min}$ and $\rho_{i,\max}$ thus generating three pairs of concentric spheres. The Cartesian workspace is then computed as the intersection of three regions, each of these corresponding to the difference between two concentric spheres. Fig. 9 shows two-

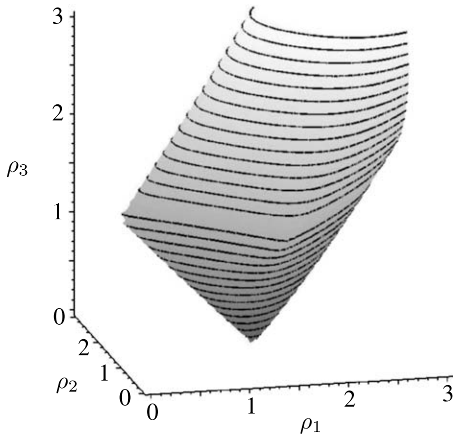

Fig. 8. Theoretical actuator workspace of the mechanism for $L = \sqrt{2}/2$.

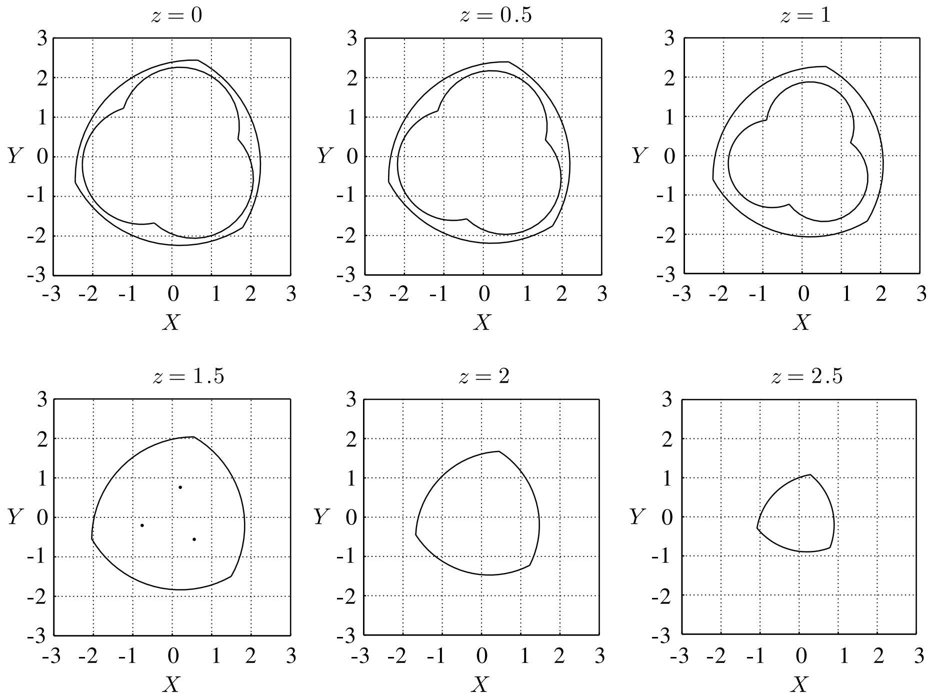

Fig. 9. Slices of the Cartesian workspace for fixed values of z with $L = \sqrt{2}/2$, $\rho_{i,\min} = 1.5$ and $\rho_{i,\max} = 3$.

dimensional slices of the mechanism's Cartesian workspace for varying values of z with $L = \sqrt{2}/2$, $\rho_{i,\min} = 1.5$ and $\rho_{i,\max} = 3$. It can be seen that the workspace consists of a single volume that has an inner core for small z. The volume of the workspace can be estimated by summing the products of the areas of each slice computed with the Gauss Divergence Theorem [29] with the Δz separating these slices. Using $\Delta z = 0.01$, this yields a volume of approximately 70 cubic units for the example shown in Fig. 9. The workspace of the mechanism is thus relatively large.

4.7. Internal forces

The prestress that is introduced in a tensegrity mechanism leads to corresponding tensile or compressive forces in its components. The magnitude of these internal forces must be considered during the design of the mechanism. In the absence of external and gravitational loads, these forces can be computed relatively easily. The first step in doing so is to compute the Cartesian coordinates of the mechanism's A_i and C_i nodes by using the analytical solution to its direct static problem. Afterwards, by summing the forces at the nodes, it is possible to determine the internal forces present in the actuators and cables. The compressive forces acting on the actuators are thus found as:

$$f_{\rho_i} = K\rho_i \tag{39}$$

while the tensile forces in the cables are

$$f_{c_i} = \frac{\sqrt{3}}{3}KL \tag{40}$$

Two important observations can be made from these results. The first is that the forces in the actuators are linear relative to both the spring stiffness and the prismatic actuator lengths. The second observation is that the tensile forces in the cables are always constant. This demonstrates the fact that, under the specified conditions, the mechanism's components are always subjected to either tensile or compressive forces.

4.8. Proof of validity for analytical solutions

All of the results given so far in Section 4 are based on the hypothesis that in the absence of external and gravitational loads the mechanism's equilibrium configurations always correspond to translations of its effector relative to its base. Furthermore, the A_i nodes forming the base of the mechanism form equilateral triangles with sides of length L. Under these assumptions, analytical solutions to the direct and inverse static problems of the mechanism were developed. However, these hypotheses were never formally proven to be valid for all sets of actuator positions. This is done in what follows.

The approach used here is to show that the analytical solution to the direct static problem of the mechanism always leads to configurations of minimal potential energy. In order to accomplish this, the potential energy must first be expressed using a minimal number of generalized coordinates representing the configuration of the mechanism so as to avoid the need for geometric constraints. As a consequence, vector $\boldsymbol{q}$ from Section 2 cannot be used. As an alternative, the mechanism can be viewed in an inverted configuration. In this way, the effector, which is formed by nodes C_i joined together with the cables of length L, now becomes the base of the mechanism. Since the attachment points of the prismatic actuators to nodes C_i of the mechanism are now fixed relative to the base, the latter can be seen as a system having six unconstrained degrees of freedom corresponding to two rotations of each prismatic actuator with respect to nodes C_i. The general configuration of the mechanism is thus represented by the ρ_i along with the following modified vector of generalized coordinates:

$$\boldsymbol{q}_m = [\alpha_{1m},\ \beta_{1m},\ \alpha_{2m},\ \beta_{2m},\ \alpha_{3m},\ \beta_{3m}]^{\mathrm{T}} \tag{41}$$

where angles α_{im} and β_{im} represent the rotations of each actuator relative to the base frame. Unit vectors directed along the prismatic actuators from nodes C_i to A_i are expressed as:

$$\boldsymbol{e}_{im} = [-\sin\beta_{im},\ \cos\alpha_{im}\cos\beta_{im},\ \sin\alpha_{im}\cos\beta_{im}]^{\mathrm{T}} \tag{42}$$

from which the positions of nodes A_i can be computed as:

$$\boldsymbol{a}_{im} = \boldsymbol{c}_{im} + \rho_i\boldsymbol{e}_{im} \tag{43}$$

with:

$$\boldsymbol{c}_{1m} = \begin{bmatrix} -L/2 \\ -\sqrt{3}L/6 \\ 0 \end{bmatrix} \quad \boldsymbol{c}_{2m} = \begin{bmatrix} L/2 \\ -\sqrt{3}L/6 \\ 0 \end{bmatrix} \quad \boldsymbol{c}_{3m} = \begin{bmatrix} 0 \\ \sqrt{3}L/3 \\ 0 \end{bmatrix} \tag{44}$$

The potential energy of the mechanism is computed using Eq. (11) with $g = 0$. The condition for the existence of critical points in the potential energy function of the mechanism is expressed as:

$$\frac{\partial U}{\partial \boldsymbol{q}_m} = \mathbf{0} \tag{45}$$

This last equation represents a system of six equations in six unknowns. In order for the critical points of the potential energy function to correspond to local minimums, the Hessian matrix ($\mathbf{H}$) of the system must be positive definite. The elements of $\mathbf{H}$ are defined as:

$$H_{rs} = \frac{\partial^2 U}{\partial q_{m,r}\partial q_{m,s}} \tag{46}$$

where $r = 1, 2, \ldots, 6, s = 1, 2, \ldots, 6, H_{rs}$ is the element located on the rth row and the sth column of $\mathbf{H}$ and while $q_{m,r}$ and $q_{m,s}$ are the rth and sth elements of $\boldsymbol{q}_m$, respectively. In order for $\mathbf{H}$ to be positive definite, the following conditions need to be satisfied:

$$\det \mathbf{H}_I > 0 \tag{47}$$

where $\mathbf{H}_I$ is the Ith upper-left submatrix of $\mathbf{H}$. In order to verify that the conditions specified by Eq. (47) are satisfied, the sines and cosines of α_{im} and β_{im} in $\mathbf{H}$ are substituted by expressions generated using the solution to the direct static problem (Eqs. (22)–(24)). This yields the following determinants that must always be positive:

$$\det \mathbf{H}_1 = -\frac{\left(2\sqrt{3}+3\right)KN_1N_2}{36L^2} \tag{48}$$

$$\det \mathbf{H}_2 = -\frac{\left(2+\sqrt{3}\right)K^2\rho_1^2N_1N_2}{18L^2} \tag{49}$$

$$\det \mathbf{H}_3 = \frac{\left(7\sqrt{3}+12\right)K^3N_1N_2N_3}{1296L^4} \tag{50}$$

$$\det \mathbf{H}_4 = -\frac{\left(362+209\sqrt{3}\right)K^4N_1N_2N_4N_5N_6N_7}{3456L^4} \tag{51}$$

$$\det \mathbf{H}_5 = -\frac{\left(6393+3691\sqrt{3}\right)K^5N_1N_2N_6N_7N_8N_9}{10368L^4} \tag{52}$$

$$\det \mathbf{H}_6 = \frac{\left(1351+780\sqrt{3}\right)K^6N_1N_2N_6N_7N_8N_{10}N_{11}}{13824L^4} \tag{53}$$

with:

$$N_1 = \left[2L + \left(2\sqrt{3}-6\right)\rho_1\right]L + \left(4-2\sqrt{3}\right)\rho_1^2 + \left(1-\sqrt{3}\right)\rho_2^2 + \left(3\sqrt{3}-5\right)\rho_3^2 \tag{54}$$

$$N_2 = \left[2L - \left(2\sqrt{3}-6\right)\rho_1\right]L + \left(4-2\sqrt{3}\right)\rho_1^2 + \left(1-\sqrt{3}\right)\rho_2^2 + \left(3\sqrt{3}-5\right)\rho_3^2 \tag{55}$$

$$\begin{aligned} N_3 = {} & L^6 + \left[4\left(1+\sqrt{3}\right)\rho_1^2 + \left(\sqrt{3}-2\right)(\rho_2^2+\rho_3^2)\right]L^4 - \left[\left(13-10\sqrt{3}\right)\rho_1^4 + \left(7-4\sqrt{3}\right)(\rho_2^4+\rho_3^4)\right. \\ & \left. + \left(40\sqrt{3}-73\right)\rho_1^2\rho_2^2 + \left(10\sqrt{3}-19\right)\rho_1^2\rho_3^2 + \left(4\sqrt{3}-7\right)\rho_2^2\rho_3^2)\right]L^2 \\ & - \frac{3}{2}\left(4\sqrt{3}-7\right)\left[2\rho_1^2 - \left(1+\sqrt{3}\right)\rho_2^2 + \left(\sqrt{3}-1\right)\rho_3^2\right]^2\rho_1^2 \end{aligned} \tag{56}$$

$$N_4 = \left(\sqrt{3}-2\right)(\rho_1^2+\rho_2^2) + \left(4\sqrt{3}-8\right)\rho_1\rho_2 + L^2 \tag{57}$$

$$N_5 = \left(\sqrt{3}-2\right)(\rho_1^2+\rho_2^2) - \left(4\sqrt{3}-8\right)\rho_1\rho_2 + L^2 \tag{58}$$

$$N_6 = \left(5-3\sqrt{3}\right)\rho_1^2 + \left(2-\sqrt{3}\right)\rho_2^2 + \left(4\sqrt{3}-7\right)\rho_3^2 + \left[L + \left(4\sqrt{3}-6\right)\rho_2\right]L \tag{59}$$

$$N_7 = \left(5-3\sqrt{3}\right)\rho_1^2 + \left(2-\sqrt{3}\right)\rho_2^2 + \left(4\sqrt{3}-7\right)\rho_3^2 + \left[L - \left(4\sqrt{3}-6\right)\rho_2\right]L \tag{60}$$

$$N_8 = L^4 + \left(\sqrt{3}-2\right)L^2\sum_{i=1}^{3}\rho_i^2 - \left(4\sqrt{3}-7\right)\left(\sum_{i=1}^{3}\rho_i^4 - \rho_1^2\rho_2^2 - \rho_1^2\rho_3^2 - \rho_2^2\rho_3^2\right) \tag{61}$$

$$N_9 = L^2 + \left(7\sqrt{3}-12\right)\rho_1^2 + \left(2\sqrt{3}-3\right)\rho_2^2 \tag{62}$$

$$N_{10} = L^2 + \left(\sqrt{3}-1\right)\rho_1^2 - \rho_2^2 + \left(2-\sqrt{3}\right)\rho_3^2 - 2\sqrt{3}L\rho_3 \tag{63}$$

$$N_{11} = L^2 + \left(\sqrt{3}-1\right)\rho_1^2 - \rho_2^2 + \left(2-\sqrt{3}\right)\rho_3^2 + 2\sqrt{3}L\rho_3 \tag{64}$$

Evaluating Eqs. (54)–(64) at a reference configuration located in the actuator workspace (e.g. $\rho_1 = \rho_2 = \rho_3 = 2$ with $L = \sqrt{2}/2$) yields the following:

$$\begin{array}{lll} N_1 < 0 & N_5 > 0 & N_9 > 0 \\ N_2 > 0 & N_6 > 0 & N_{10} < 0 \\ N_3 < 0 & N_7 < 0 & N_{11} > 0 \\ N_4 < 0 & N_8 < 0 & \end{array} \tag{65}$$

Referring to Eqs. (48)–(53), it can thus be seen that the condition given by Eq. (47) is satisfied in this configuration. For the sign of N_9 to change within the workspace, it must at some point become zero. The solution of N_9 for ρ_2 is:

$$\rho_2 = \sqrt{-4\left(2\sqrt{3}-3\right)\left[L^2+\left(7\sqrt{3}-12\right)\rho_1^2\right]} \tag{66}$$

Since the term appearing in the square root is always negative, it is clear that N_9 can never be equal to zero which implies that $N_9 > 0$ at all times. A graphical approach is used to prove that the signs of the remaining N_i expressions do not change inside the workspace. For each N_i, the corresponding surface is plotted along with the boundary of the mechanism's actuator workspace. By visually inspecting the position of the surface relative to the workspace boundary, it can be observed that none of the surfaces penetrate the workspace. Because of this, the results given in Eq. (65) are valid throughout the workspace and so is the solution to the direct static problem given in Section 4.1.

5. Conclusion

In this paper, the kinematics and statics of a spatial tensegrity mechanism were analysed. Tensegrity mechanisms benefit from the fact that all of their components are subjected to either tensile or compressive forces. As a consequence, cables and springs can be used extensively thus reducing the mechanism's inertia.

By performing a mobility analysis of the mechanism, it was found that it has unconstrained degrees of freedom. This property adds complexity to the computation of the mechanism's equilibrium configurations. In fact, a numerical approach based on a minimization of the mechanism's potential energy is required for solving the direct and inverse static problems. By modifying the positions of the actuators, the equilibrium configurations of the mechanism can be controlled with three degrees of freedom.

The presence of unconstrained degrees of freedom allows the mechanism to deform under the application of external loads. The extent with which the mechanism is able to support external loads without losing its stability or the tension in its cables was quantified by the set of allowable external forces. For a given configuration, it was shown that the mechanism has a considerably higher resistance for loads that tend to *extend* it. Since the set of allowable forces is configuration dependent, a more complete analysis spanning the workspace of the mechanism would be required in order to reach general conclusions.

For a special case where external and gravitational loads are not considered, analytical solutions to the direct and inverse static problems were found. Interestingly, under these assumptions, the mechanism is purely translational. The analytical solutions were subsequently used to compute the actuator and Cartesian workspaces of the mechanism that were found to be relatively large when compared to its physical size.

It was mentioned in Section 2 that the triangular tensegrity prism has instantaneous mobility allowing it to deform slightly without requiring modifications to the lengths of its components. Although the analysis of the mechanism's dynamics was not discussed here, it can be shown that its instantaneous mobility leads to vibrations about its equilibrium configurations which must be suppressed using dampers. Alternatively, as was explained by Knight [30], it is possible to use additional tensile components in order to generate reinforced tensegrity prisms that do not have instantaneous mobility. These extra components lead to an improved performance of the mechanism with respect to its dynamics, its resistance to external loads and its stiffness. The dynamic simulation of the reinforced system was dealt with in [31].

Acknowledgements

The authors wish to thank the Natural Sciences and Engineering Research Council of Canada (NSERC) for their financial support as well as the Fonds Québécois de la Recherche sur la Nature et les Technologies (FQRNT) and the Canada Research Chair Program (CRC).

References

[1] D.G. Emmerich, Structures tendues et autotendantes, in: Monographies de Géometrie Constructive, Éditions de l'École d'Architecture de Paris La Villette, Paris, France, 1988.
[2] B. Fuller, Synergetics: The geometry of thinking, MacMillan Publishing Co., Inc., New York, USA, 1975.
[3] R. Motro, Tensegrity systems: the state of the art, International Journal of Space Structures 7 (2) (1992) 75–83.
[4] A. Pugh, An Introduction to Tensegrity, first ed., Berkeley: University of California Press, Los Angeles, California, USA, 1976.

[5] G. Tibert, Deployable tensegrity structures for space applications, Ph.D. Thesis, Department of Mechanics, Royal Institute of Technology, Stockholm, Sweden, 2002.
[6] H. Furuya, Concept of deployable tensegrity structures in space applications, International Journal of Space Structures 7 (2) (1992) 143–152.
[7] S. Pellegrino, Analysis of prestressed mechanisms, International Journal of Solids and Structures 26 (12) (1990) 1329–1350.
[8] K. Kebiche, M. Kazi-Aoual, R. Motro, Geometrical non-linear analysis of tensegrity systems, Engineering Structures 21 (9) (1999) 864–876.
[9] C.D. Crane III, J. Duffy, J.C. Correa, Static analysis of tensegrity structures. Part 1. Equilibrium equations, in: Proceedings of the 2002 ASME Design Engineering Technical Conference, Montréal, Québec, Canada, 2002, pp. 671–680.
[10] D. Williamson, R. Skelton, J. Han, Equilibrium conditions of a tensegrity structure, International Journal of Solids and Structures 40 (23) (2003) 6347–6367.
[11] R. Skelton, Dynamics and control of tensegrity systems, in: IUTAM Symposium on Vibration Control of Nonlinear Mechanisms and Structures, Munich, Germany, 2005.
[12] J. Bayat, C.D. Crane III, Closed-form equilibrium analysis of a planar tensegrity structure, in: Proceedings of the ninth International Symposium on Advances in Robot Kinematics, Liguria, Italy, 2004.
[13] C. Sultan, M. Corless, R. Skelton, The prestressability problem of tensegrity structures: some analytical solutions, International Journal of Solids and Structures 38 (30) (2001) 5223–5252.
[14] A.G. Tibert, S. Pellegrino, Review of form-finding methods for tensegrity structures, International Journal of Space Structures 18 (4) (2003) 209–223.
[15] R.E. Skelton, R. Adhikari, J.-P. Pinaud, W. Chan, J.W. Helton, An introduction to the mechanics of tensegrity structures, in: Proceedings of the IEEE Conference on Decision and Control, Orlando, Florida, USA, 2001, vol. 5, pp. 4254–4259.
[16] I.J. Oppenheim, W.O. Williams, Geometric effects in an elastic tensegrity structure, Journal of Elasticity 59 (1) (2000) 51–65.
[17] I.J. Oppenheim, W.O. Williams, Tensegrity prisms as adaptive structures, ASME Adaptive Structures and Material Systems 54 (1997) 113–120.
[18] M. Marshall, C.D. Crane III, Design and analysis of a hybrid parallel platform that incorporates tensegrity, in: Proceedings of the ASME 2004 Design Engineering Technical Conferences and Computers and Information in Engineering Conference, Salt Lake City, Utah, USA, 2004, pp. 535–540.
[19] C. Sultan, M. Corless, Tensegrity flight simulator, Journal of Guidance, Control, and Dynamics 23 (6) (2000) 1055–1064.
[20] C. Sultan, M. Corless, R.E. Skelton, Peak to peak control of an adaptive tensegrity space telescope, in: Proceedings of the International Society for Optical Engineering, vol. 3667, 1999, pp. 190–201.
[21] C. Sultan, R. Skelton, A force and torque tensegrity sensor, Sensors and Actuators, A: Physical 112 (2–3) (2004) 220–231.
[22] M. Arsenault, C. Gosselin, Kinematic, static and dynamic analysis of a planar 1-DoF tensegrity mechanism, ASME Journal of Mechanical Design 127 (6) (2005) 1152–1160.
[23] M. Arsenault, C. Gosselin, Kinematic, static and dynamic analysis of a planar 2-DoF tensegrity mechanism, Mechanism and Machine Theory 41 (9) (2006) 1072–1089.
[24] M. Arsenault, C. Gosselin, Kinematic, static and dynamic analysis of a spatial three-degree-of-freedom tensegrity mechanism, ASME Journal of Mechanical Design 128 (5) (2006) 1061–1069.
[25] H. Kenner, Geodesic Math and How To Use It, first ed., University of California Press, Berkeley, California, USA, 1976.
[26] D. Streit, B. Gilmore, Perfect spring equilibrators for rotatable bodies, Journal of Mechanisms, Transmissions, and Automation in Design 111 (4) (1989) 451–458.
[27] J. Herder, Energy-free systems: theory, conception and design of statically balanced spring mechanisms, Ph.D. thesis, Delft University of Technology, Delft, Netherlands, 2001.
[28] J. Phillips, Freedom in Machinery: vol. 1, Introducing Screw Theory, Cambridge University Press, Cambridge, UK, 1984.
[29] C.M. Gosselin, Determination of the workspace of 6-DoF parallel manipulators, ASME Journal of Mechanical Design 112 (3) (1990) 331–336.
[30] B. Knight, Y. Zhang, J. Duffy, C.D. Crane III, On the line geometry of a class of tensegrity structures, in: Proceedings of a Symposium commemorating the legacy, works, and life of Sir Robert Stawell Ball, Cambridge, UK, 2000.
[31] M. Arsenault, C. Gosselin, Dynamic simulation of a spatial 3-DoF tensegrity mechanism, Transactions of the Canadian Society of Mechanical Engineering 29 (4) (2005) 491–505.